UVicSPACE: Research & Learning Repository

University of Victoria

Faculty of Science

Faculty Publications

Radiative forcing at high concentrations of well-mixed greenhouse gases

B.Byrne and C. Goldblatt

January 2014

©2013. American Geophysical Union. All Rights Reserved.

This article was originally published at:

http://dx.doi.org/10.1002/2013GL058456

Citation for this paper:

Byrne, B. & Goldblatt, C. (2014). Radiative forcing at high concentrations of well-mixed greenhouse gases. *Geophysical Research Letters*, 41(1), 152-160.

AGU PUBLICATIONS

Geophysical Research Letters

RESEARCH LETTER
10.1002/2013GL058456

Key Points:
- The IPCC expressions perform poorly at high GHG concentrations
- The new expressions provided perform much better at high GHG concentrations
- Forcings with latitude dependence are provided for forcing models

Supporting Information:
- Readme
- Atmospheric pressure, temperature, water vapor, and ozone profiles used to calculate fluxes.
- Cloud fraction, pressure level and optical depth. Each numerical row represents an atmospheric profile from top to bottom the rows represent the 00°-15°, 15°-30°, 30°-45°, 45°-60°, 60°-75°, 75°-90°, and the GAM profile.
- The atmospheric concentration of CO_2 and the resulting instantaneous radiative forcing using the radiative tropopause.
- The atmospheric concentration of CH_4 and the resulting instantaneous radiative forcing using the radiative tropopause.
- The atmospheric concentration of N_2O and the resulting instantaneous radiative forcing using the radiative tropopause.

Correspondence to:
B. Byrne,
bbyrne@uvic.ca

Citation:
Byrne, B., and C. Goldblatt (2014), Radiative forcing at high concentrations of well-mixed greenhouse gases, *Geophys. Res. Lett.*, *41*, 152–160, doi:10.1002/2013GL058456.

Received 24 OCT 2013
Accepted 15 DEC 2013
Accepted article online 18 DEC 2013
Published online 13 JAN 2014
Corrected 17 APR 2015

This article was corrected on 17 APR 2015. See end of the full text for details.

Radiative forcing at high concentrations of well-mixed greenhouse gases

B. Byrne[1] and C. Goldblatt[1]

[1]School of Earth and Ocean Sciences, University of Victoria, Victoria, British Columbia, Canada

Abstract We present new calculations of radiative forcing at very high concentrations of CO_2, CH_4, and N_2O, relevant to extreme anthropogenic climate change and paleoclimate studies. CO_2 forcing is calculated over the range 100 ppmv to 50,000 ppmv, and the maximum forcing is 38.1 W m^{-2}. CH_4 and N_2O forcings are calculated over the range 100 ppbv to 100 ppmv and give maximum forcings of 6.66 W m^{-2} and 22.3 W m^{-2}. The sensitivity of our calculations to spatial averaging and tropopause definition is examined. We compare our results with the "simplified expressions" reported by Intergovernmental Panel on Climate Change (IPCC) and find significant differences at high greenhouse gas concentrations. We provide new simplified expressions which agree much better with the calculated forcings and suggest that these expressions be used in place of the IPCC expressions. Additionally, we provide meridionally resolved forcings which may be used to force simple and intermediate complexity climate models.

1. Introduction

Radiative forcing is the change in the net flux of radiation at the tropopause due to a change in greenhouse gas concentration. Given that the tropospheric structure is determined largely by convection, it has been found that the change in surface temperature is directly proportional to the radiative forcing. Hence, this becomes the simplest way of quantifying the effect in a perturbation in greenhouse gas inventory and of comparing greenhouse gases. In this paper, we present new calculations of radiative forcing at very high concentrations of CO_2, CH_4, and N_2O, relevant to extreme anthropogenic climate change, paleoclimate studies, and models of the carbon cycle evolution.

Calculating a radiative forcing requires running a radiative transfer model for perturbed and unperturbed greenhouse gas concentrations. As these are rather specialist codes, it is very common to refer to empirical fits or "simplified expressions" of radiative forcing as given by the Intergovernmental Panel on Climate Change, first in *IPCC* [1990] and updated in *IPCC* [2001]. Using the property that change in surface temperature is proportional to radiative forcing; radiative forcings are often used to force climate models which do not have vertically resolved atmospheres, ranging from simple box models to Earth system models of intermediate complexity, e.g., the UVic model [*Weaver et al.*, 2001], the MICRO-lite model [*Tachiiri et al.*, 2010], and the DCESS Earth System Model [*Shaffer et al.*, 2008].

The existing commonly used simplified expressions [*IPCC*, 2001] were fitted for CO_2 concentrations up to 1000 ppmv and CH_4 and N_2O concentrations up to 5 ppmv [*Hansen et al.*, 1988]. However, some current anthropogenic emission scenarios project higher gas concentrations. For example, representative concentration pathway (RCP) 8.5 projects 1962 ppmv CO_2 for year 2250 [*Meinshausen et al.*, 2011]. For palaeoclimate, higher concentrations are required. The standard compilation [*Royer* 2006] of geological CO_2 proxies for 450 Ma to present shows CO_2 of 1000 to 3000 ppmv to be common and concentrations of up to 6000 ppmv to occur at times. *Beerling et al.* [2009] estimate CH_4 concentrations of 10–12 ppmv in Permo-Carboniferous. Modeling of CH_4 concentrations since 400 Ma suggests that 3 ppmv is common, with peak concentrations of 12 ppmv around the Permian-Carboniferous boundary (299 Ma). Destabilization of methane clathrates could give higher concentration still [*Schmidt and Shindell*, 2003]. Given the uncertainties in paleoconcentration estimates, we examine larger concentration ranges to bound these estimates.

In this paper, we calculate radiative forcings for CO_2 up to 50,000 ppmv and CH_4 and N_2O up to 100 ppmv at line-by-line spectral resolution, for both clear and cloudy skies. We examine the overlap between forcings and propose new simplified expressions for the forcings over the full range of concentrations we consider.

©2013. American Geophysical Union. All Rights Reserved.

We also calculate the meridional variation in forcing, which will be applicable to climate models forced with radiative forcings.

2. Methods

2.1. Radiative Transfer Calculation

We use the Spectral Mapping for Atmospheric Radiative Transfer code, written by David Crisp [*Meadows and Crisp*, 1996], for our radiative transfer calculations. This code works at line-by-line resolution but uses a spectral mapping algorithm to treat different wave number regions with similar optical properties together, giving significant savings in computational cost. We evaluate the radiative transfer in the range 50–100,000 cm^{-1} (0.1–200 μm) as a combined solar and thermal calculation.

Line data for all radiatively active gases are taken from the HITRAN 2012 database. Cross sections are taken from the NASA Astrobiology Institute Virtual Planetary Laboratory Spectral Database http://depts.washington.edu/naivpl/content/molecular-database.

2.2. Atmosphere Profiles

Appropriate averaging of the atmospheric structure is required to calculate the radiative forcing. It is important to note that a radiative forcing calculated on averaged profiles is not the same as the average radiative forcing. Temporal and zonal averaging leads to small errors (1%) in calculated radiative forcing, whereas meridional averaging gives larger errors (3% for CO_2, higher for poorly mixed gases) [*Myhre and Stordal*, 1997; *Freckleton et al.*, 1998].

We calculate mean profiles from the Modern Era Retrospective-analysis for Research and Applications reanalysis data products [*Rienecker et al.*, 2011]. The climatology is averaged zonally and temporally over the period 1979 to 2011. We used two meridional profile sets. (1) A single Global Annual Mean (GAM) and (2) 15° meridional bins, to give six profiles, the area-weighted sum of which gives a global forcing (Figure 1). Tables of profiles are available as supporting information online. Our solar source is spectrally resolved. We use solar zenith angles of 60° for the GAM profile and 51.0°, 54.1°, 60.0°, 67.0°, 75.5°, and 83.7° for the profiles in the six profile sets. These zenith angles correspond to the average intensity of insolation over the course of a day.

2.3. Cloud Climatology

Clouds absorb in the same spectral regions as the greenhouse gases we consider, so the presence of clouds will reduce the radiative forcing relative to clear sky conditions. Thus, clouds must be resolved. We take our cloud climatology as cloud fractions and optical depths from International Satellite Cloud Climatology Project D2 data set, averaging from January 1990 to December 1992. This period is used by *Rossow et al.* [2005] and was chosen so that we could compare cloud fractions. We assume random overlap and average by area to estimate cloud fractions (Figure 1). Tables of cloud properties are available as supporting information online.

2.4. Radiative Forcing Definition

Two definitions of radiative forcing are relevant to this study. The calculations performed in this study use the instantaneous radiative forcing, F_i, which is the change in net flux at the tropopause with no feedbacks. The simplified expressions given by *IPCC* [2001] are for the adjusted forcing, F_a, which is the change in net flux at the tropopause after allowing stratospheric temperatures to adjust to equilibrium. The reason for allowing stratospheric adjustment is that the stratosphere adjusts to a radiative perturbation rapidly (months) in comparison to the troposphere (decades) which is tightly coupled to the ocean. Therefore, F_a should be expected to be a better measure of the expected climate response for long lasting forcings than F_i.

However, calculating F_a is much more computationally expensive than calculating F_i, requiring iterative calculation of stratospheric adjustment. To be confident in the accuracy of the calculated forcings, we use a model which is very computationally expensive. The trade off is that the computational cost of calculating F_a would be prohibitive. Calculating F_i allows us to supply reference flux profiles, against which faster models may be tested for future work calculating F_a.

The difference in F_i and F_a from *Hansen et al.* [2005] can be used to bound the expected uncertainty from only calculating F_i here. The difference is largest for CO_2, which cools the stratosphere. F_i is larger than F_a by

©2013. American Geophysical Union. All Rights Reserved.

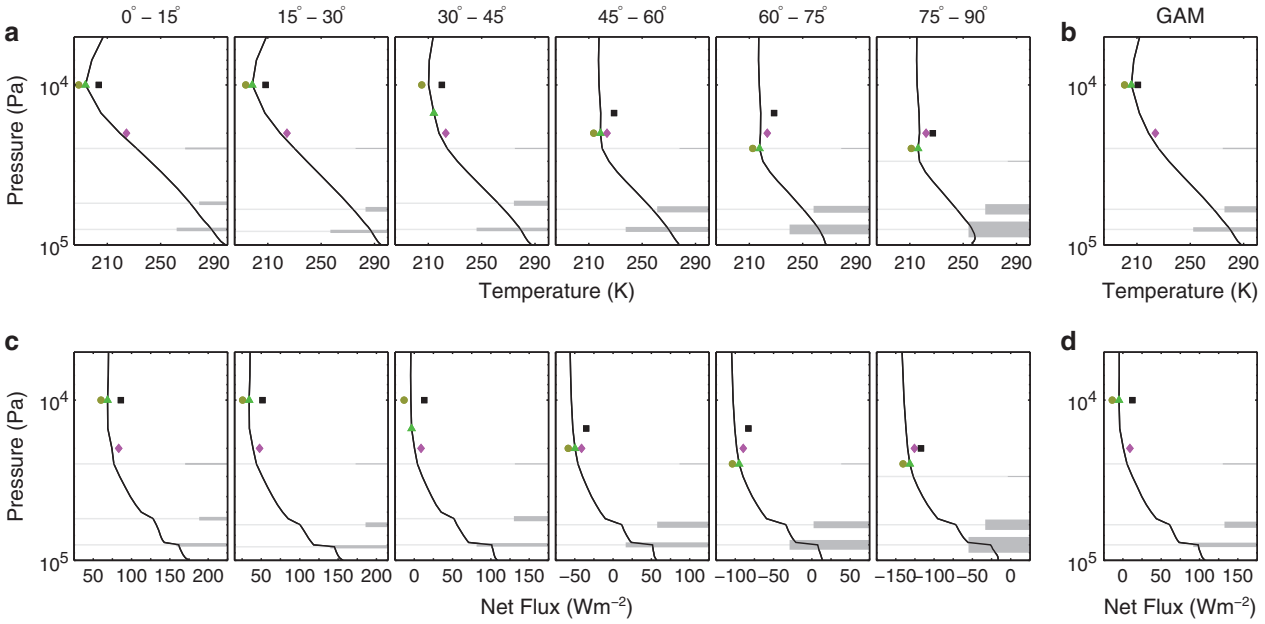

Figure 1. Atmospheric profiles. Temperature structure of the atmosphere for (a) six profile sets and (b) GAM profile and net flux profile at pre-industrial gas concentrations for (c) six profile sets and (d) GAM profile. For all panels, the grey lines represent cloud height, line thickness indicates the cloud optical thickness, and the width of the thick line corresponds to cloud fraction. Markers represent tropopause height for each tropopause: temperature minimum (yellow circle), lapse rate (green triangle), 200 hPa (magenta diamond), and radiative (black square).

10% for a small increase in CO_2 from reference conditions (for which the magnitude of the radiative forcing is small), 7.5% larger at 8 $\times$ CO_2 (2328 ppmv), and the difference is expected to decrease further for the higher CO_2 which we focus on. For CH_4 and N_2O, the maximum differences are 4.5% and 2.5%, respectively.

2.5. Tropopause Definition

The tropopause is the boundary between the troposphere and the stratosphere. It is commonly seen as the base of the stratospheric temperature inversion. However, from a radiative perspective, relevant here, the inversion is somewhat a coincidence (due to the particularly high strength of UV absorption by ozone).

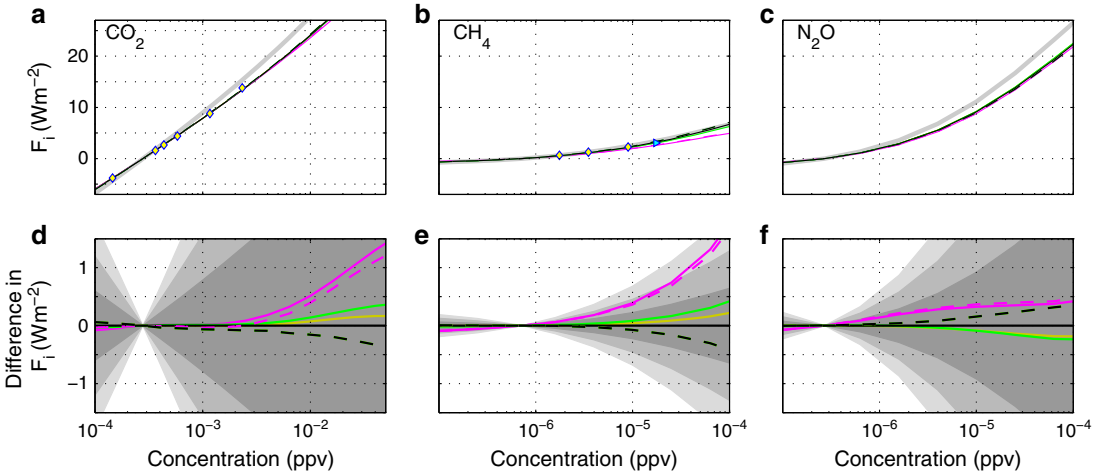

Figure 2. Radiative forcings. (a–c) Calculated radiative forcing for each gas with various tropopause definitions. Colored lines are all-sky forcings: yellow for temperature minimum, green for lapse rate, magenta for 200 hPa and black for radiative, solid lines from six profile sets, and dashed from GAM. Grey line is clear-sky radiative forcing for six profiles radiative tropopause. The yellow diamonds represent the all-sky F_o from *Hansen et al.* [2005], and cyan triangle represent clear-sky F_i from *Kurten et al.* [2011], included for comparison. (d–f) Difference in radiative forcing between each tropopause definition and the radiative tropopause definition. Colors are the same as in the top row (note that lapse rate, temperature, and radiative definitions are coincident for the GAM profile). Shading represents the percentage difference in radiative forcings, from dark grey to white of 0–10%, 10–20%, 20–30%, and greater than 30%.

©2013. American Geophysical Union. All Rights Reserved.

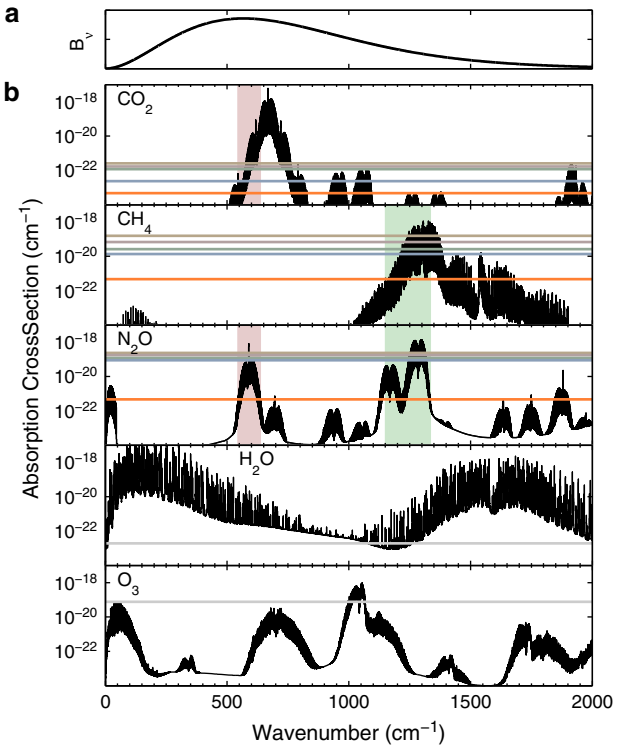

Figure 3. Absorption cross sections. (a) Spectral radiance (B_ν) emitted by a blackbody of 289 K, for reference. (b) Representative absorption cross sections for each greenhouse gas (calculated for 500 hPa and 260 K). Horizontal lines are the absorption cross section at which the optical depth due to that gas would be unity over the entire atmosphere, given some concentration or column abundance of the gas. Reference gas concentrations: glacial minimum (pastel yellow), pre-industrial (pastel red), present day (pastel green), and RCP 8.5 year 2250 (pastel blue). Orange is the maximum concentration we consider for each greenhouse gas. For water and ozone, grey lines correspond to column abundance for GAM profile. Shaded areas highlight gas overlap; pink for CO_2–N_2O and green for CH_4–N_2O.

Our primary concern is the transition from the troposphere temperature structure dominated by large-scale air motions and the stratosphere which is largely in radiative equilibrium. Defining the tropopause as the lowest level which is in radiative equilibrium, surface temperature change being proportional to radiative forcing follows directly.

However, the tropopause height varies spatially (higher in tropics) and temporally, so averaging introduces inherent ambiguity in the tropopause height. When a prescribed tropopause definition is used in F_a calculations, different definitions lead to 10% variation in F_a calculations [*Myhre and Stordal*, 1997], comparable to the difference between F_a and F_i.

An advantage of calculating F_i from fixed profiles is we can easily compare different tropopause definitions. We compare (1) the level at which the lapse rate changes sign (temperature minimum tropopause); (2) the lowest level at which the temperature lapse rate between this and all higher levels within 2 km falls bellow 2 K km^{-1} (lapse rate tropopause) [*WMO*, 1986]; (3) the 200 hPa pressure level (200 hPa pseudotropopause) [*Collins et al.*, 2006]; and (4) the lowest level at which the difference in net flux between this level and the next higher level is below an arbitrary threshold, taken as 3 W m^{-2} here (radiative tropopause) (Figure 1).

3. Results

3.1. Calculated Forcings

We calculated radiative forcings for CO_2, CH_4, and N_2O on the GAM profile and the six profile sets (Figure 2). We take the radiative definition of the tropopause on the six profile sets to be the most physically realistic and use this as reference for comparison. For all gases, the 200 hPa pseudotropopause gives the largest error relative to the reference; we do not recommend this for radiative forcing calculations. In all other cases, the difference in F_i due to different tropopause definitions is less than 1 W m^{-2}. For the six profile sets, the largest percentage differences are 0.9%, 6.8%, and 1.7% for CO_2, CH_4, and N_2O, respectively. For the GAM, all

©2013. American Geophysical Union. All Rights Reserved.

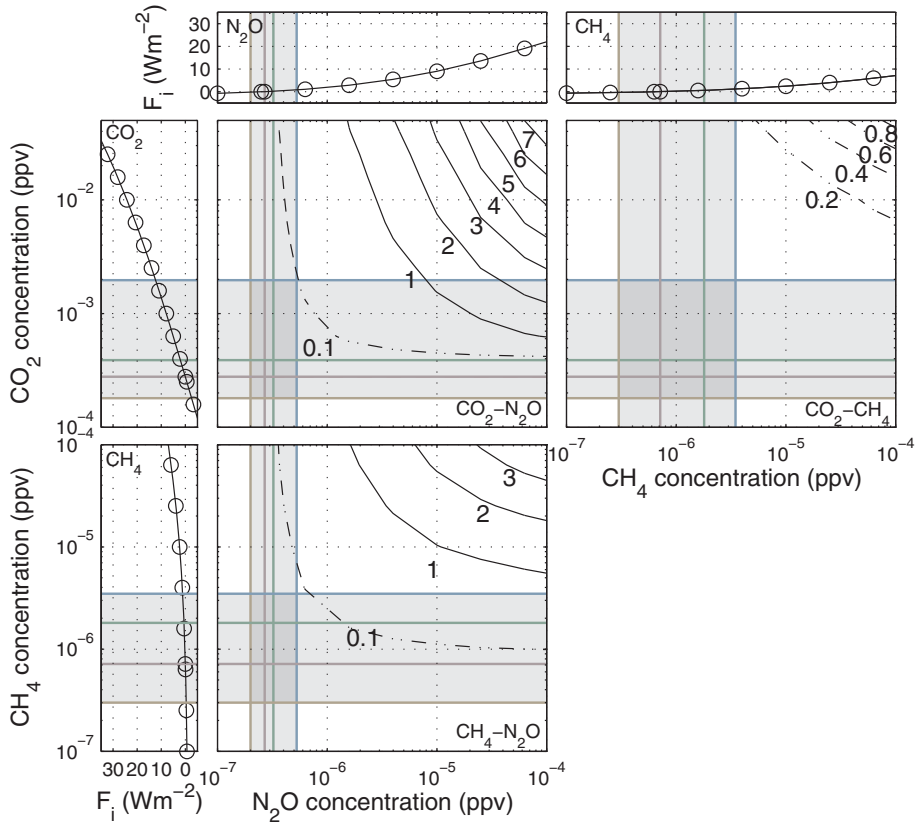

Figure 4. Reduction in F_i due to overlap. Peripheral line plots are radiative forcing for each gas, for reference. Contour plots show the reductions in radiative forcing due to overlapping absorption (W m^{-2}) for (bottom) CH_4–N_2O, (top, left) CO_2–N_2O, and (top right) CO_2–CH_4. Contours are solid for reductions in radiative forcing greater than 1 W m^{-2} and dash-dotted for less that 1 W m^{-2}. Vertical and horizontal pastel lines are reference concentrations, colors as in Figure 3.

tropopause definitions are coincident, and the error (maximum 1.0%, 6.9%, and 1.2% for CO_2, CH_4, and N_2O, respectively) arises from meridional averaging. The largest discrepancies are for CH_4 which is a good solar absorber at higher concentrations. Solar radiation is absorbed around the tropopause, so small differences in the vertical position of the tropopause strongly affect the net flux.

3.2. Overlap

When multiple gases absorb radiation at the same frequencies, the total absorption (and hence radiative forcing) is less than the sum of the absorptions that each gas would contribute in isolation. This difference is known as overlap. It occurs because the absorption is distributed between the gases, so in effect there is less radiation available for each gas to absorb.

Table 1. IPCC Radiative Forcing Fits[a]

Gas	Expression	Constants	Based On
CO_2	$F_a = \alpha \ln (C/C_0)$	$\alpha = 5.35$	*IPCC* [1990]
	$F_a = \alpha \ln (C/C_0) + \beta \left(\sqrt{(C)} - \sqrt{(C_0)} \right)$	$\alpha = 4.841,\ \beta = 0.0906$	*Shi* [1992]
	$F_a = \alpha (g(C) - g(C_0))$	$\alpha = 3.35$	*WMO* [1999]
	where $g(C) = \ln (1 + 1.2C + 0.005C^2 + 1.4 \times 10^{-6} C^3)$		
CH_4	$F_a = \alpha \left(\sqrt{(M)} - \sqrt{(M_0)} \right) - (f(M, N_0) - f(M_0, N_0))$	$\alpha = 0.036$	*IPCC* [1990]
N_2O	$F_a = \alpha \left(\sqrt{(N)} - \sqrt{(N_0)} \right) - (f(M_0, N) - f(M_0, N_0))$	$\alpha = 0.12$	*IPCC* [1990]
	$f(M, N) = 0.47 \ln [1 + 2.01 \times 10^{-5} (MN)^{0.75} + 5.31 \times 10^{-15} M (MN)^{1.52}]$		

[a]The simplified expressions of radiative forcing are given in *IPCC* [2001]. C is CO_2 in ppmv, M is CH_4 in ppbv, and N is N_2O in ppbv.

©2013. American Geophysical Union. All Rights Reserved.

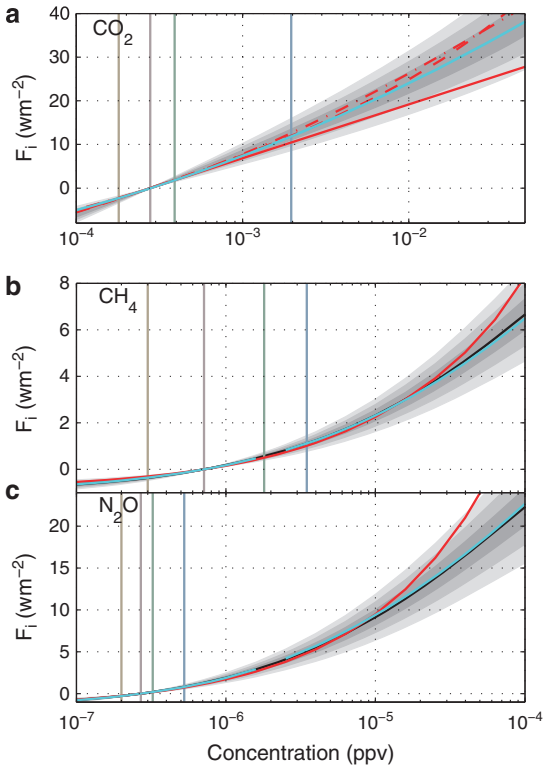

Figure 5. Simplified expressions for radiative forcings. Fits to radiative forcing for (a) CO_2, (b) CH_4, and (c) N_2O. For all panels, black line is our calculated radiative forcing for six profiles radiative tropopause, cyan line is our new fit, and red lines are *IPCC* [2001] simplified expressions (dashed based on *IPCC* [1990]), dash-dotted based on *Shi* [1992] and solid based on *WMO* [1999]. Vertical lines are reference concentrations, in color, as in Figure 3. Shaded regions correspond to amount of error, as in Figure 2.

Figure 3 shows the absorption cross sections of the main greenhouse gases and highlights overlapping absorption. N_2O–CO_2 overlap occurs around 600 cm^{-1}. Over the N_2O concentrations expected due to anthropogenic emissions this absorption feature is not optically thick, so the reduction in F_i is expected to be small. However, at higher N_2O concentrations the overlap becomes increasingly important as this absorption feature becomes optically thick. N_2O–CH_4 overlap occurs between 1150 and 1350 cm^{-1}, the spectral range at which both N_2O and CH_4 absorb best, so there will be a significant overlap effect. There is minimal overlap between CO_2 and CH_4.

Reduction in radiative forcing due to overlap is shown in Figure 4. For all gases, where concentration is less than RCP 8.5 year 2250 concentrations, the effect of overlap is small (< 0.1 W m^{-2}). However, N_2O–CH_4 and

Table 2. New Radiative Forcing Fits[a]

Gas	Simplified Expression	Concentration (ppmv)
CO_2	$F_i = 5.32 \ln(C/C_0) + 0.39[\ln(C/C_0)]^2$	200–10,000
CH_4	$F_i = 1173\left(\sqrt{(M)} - \sqrt{(M_0)}\right) - 71,636\left(\sqrt{(M)} - \sqrt{(M_0)}\right)^2$	0.1–2.5
	$F_i = 0.824 + \frac{4}{5}\ln(M/M_1) + \frac{1}{5}[\ln(M/M_1)]^2$	2.5–100
N_2O	$F_i = 3899(\sqrt{(N)} - \sqrt{(N_0)}) + 38,256(\sqrt{(N)} - \sqrt{(N_0)})^2$	0.1–2.5
	$F_i = 4.182 + 3\ln(N/N_1) + 0.5469[\ln(N/N_1)]^2$	2.5–100
N_2O–CO_2 overlap	$\Delta F_i = -16.16 \exp(-0.036(\ln(C - C_0) - 0.0024)^2 - 0.05(\ln(N - N_0) + 6.5)^2)$	
N_2O–CH_4 overlap	$\Delta F_i = -24 \exp(-0.02(\ln(M - M_0) - 0.01)^2 - 0.044(\ln(N - N_0) + 7.73)^2)$	

[a]Simplified expressions fit to calculated radiative forcings. C, M, and N represent the concentrations of CO_2, CH_4, and N_2O in ppv. $C_0 = 278\times10^{-6}$, $M_0 = 715\times10^{-9}$, $N_0 = 270\times10^{-9}$, and $N_1 = M_1 = 2.5\times10^{-6}$. All radiative forcings are given from pre-industrial concentrations. N_2O–CO_2 and N_2O–CH_4 overlaps are the reductions in radiative forcing due to overlapping absorption.

©2013. American Geophysical Union. All Rights Reserved.

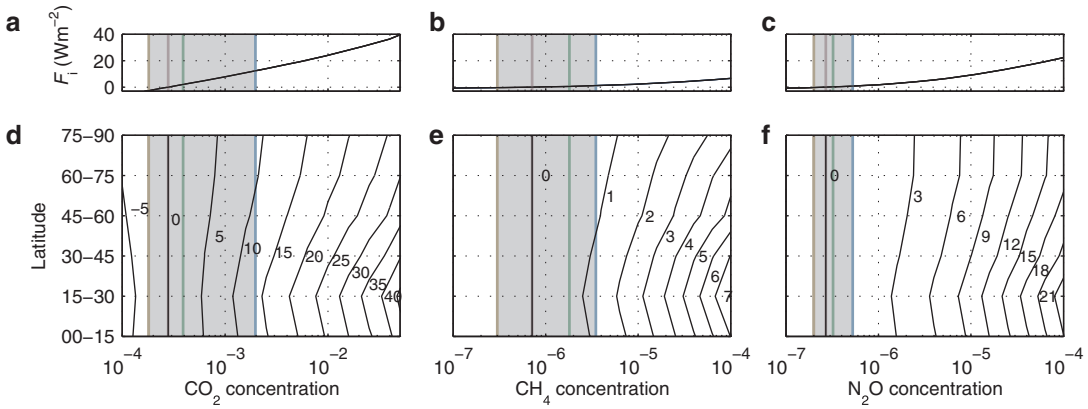

Figure 6. Calculated F_i as a function of concentration and latitude. Mean radiative forcing for (a) CO_2, (b) CH_4, and (c) N_2O and latitude-dependent forcing for (d) CO_2, (e) CH_4, and (f) N_2O. Vertical lines are reference concentrations, colors as in Figure 2.

N_2O–CO_2 overlaps become important (several W m^{-2}) at higher concentrations and should be accounted for in any applications.

3.3. IPCC Fits

The family of simplified fits from *IPCC* [2001] are summarized in Table 1 and compared to our new F_i calculations in Figure 5. There are various legitimate reasons for there to be a discrepancy between calculated forcings, as discussed above. Conservatively, we take forcings within 10% to be in agreement.

For CO_2, there are three simplified expressions in *IPCC* [2001]. The fit based on *WMO* [1999] is in very close agreement with our new calculations. The fit based on *Shi* [1992] is in less close agreement, but still within 10%. However, the fit based on *IPCC* [1990] is in poor agreement with our calculated F_i above 1000 ppmv, underestimating the radiative forcing, so we do not recommend this for high CO_2 concentrations. We note, however, that this is the most commonly used fit.

For CH_4, the shape of the curve from the IPCC fit is somewhat different from our calculated F_i, though the absolute differences (in W m^{-2}) are small as CH_4 is a weak greenhouse gas. Divergence becomes large at 20 ppmv, with the radiative forcing overestimated by the IPCC fit. For N_2O, the IPCC fit is in good agreement with our calculated F_i up to 10 ppmv, above which it strongly overestimates the radiative forcing. Thus use of the IPCC fits for CH_4 and N_2O for high greenhouse gas concentrations are not recommended.

3.4. New Fits

We propose new simplified expressions for radiative forcings for individual gases (Table 2). Theoretically, the relationship between radiative forcing and concentration should be linear at low concentrations, square root at intermediate concentrations, and logarithmic at high concentrations. These approximate relationships come from the shape of absorption lines. When the entire line is optically thin, increasing the greenhouse gas concentration causes a linear increase in the radiative forcing. As the concentration increases, the line center becomes saturated and most additional absorption happens in the wings, the shape of which gives a square root dependence on concentration. As the lines become saturated further out, the absorption becomes logarithmic with concentration. Of course, many lines contribute to absorption, not just one, but as dominant absorption is generally in one of the three categories, these approximations work reasonably well over large ranges of concentration. For CO_2, the concentration range of interest is all within the logarithmic regime, so a single fit is given. For CH_4 and N_2O, the range of interest of concentrations straddles the square root and logarithmic regimes, so separate fits are proposed for concentrations above and below 2.5 ppmv.

For gas concentrations beyond RCP 8.5 year 2250 projections, accounting for overlap is necessary. In Table 2, we supply new fits for the overlap, which should be subtracted from the sum of the individual gas forcings.

3.5. Meridional Variation in F_i

The radiative forcings described so far are for global annual mean conditions, but at high greenhouse gas concentrations the forcing varies by several W m^{-2} between the tropics and the poles (Figure 6). These meridional variations in the radiative forcing are primarily caused by variations in surface temperature and

©2013. American Geophysical Union. All Rights Reserved.

atmospheric water vapor concentrations, though differences in cloud climatology, tropopause height, and insolation also contribute.

The simplified expressions from *IPCC* [2001], which are for global annual mean conditions, are commonly used to force spatially resolved models [e.g., *Weaver et al.*, 2001] at each grid cell, failing to account for these meridional variations. *Hansen et al.* [1997] applied a "ghost" forcing of 8 W m^{-2} to the surface either poleward or equatorward of 30°, resulting in temperature differences of 4.39°C and 2.37°C, respectively. Clearly, the climate response has a substantial dependence on the meridional distribution of the forcing.

It is not practical to develop simplified expressions for meridionally resolved forcings. As an alternative, we supply a table of these in the online supporting information and recommend these be used with appropriate interpolation to force spatially resolved models.

4. Conclusions

We have performed new radiative forcing calculations for high concentrations of CO_2, CH_4, and N_2O appropriate for extreme anthropogenic global warming and paleoclimate studies. We provide simplified fits to these radiative forcings which are recommended in place of those from *IPCC* [2001] for high greenhouse gas concentrations. The reduction in radiative forcings due to overlap between these gases is less than 0.1 W m^{-2} for concentrations up to RCP 8.5 year 2250 values. For larger concentrations, N_2O–CH_4 and N_2O–CO_2 overlap can reduce the radiative forcing by several W m^{-2}. We also provide simplified fits to account for this overlap. One should also note that additional products of atmospheric chemistry have radiative effects [*IPCC*, 2013], but these are not considered here.

The difference in radiative forcing between the tropics and the poles is considerable and increases with the magnitude of radiative forcing (e.g., the meridional variation in forcing increases monotonically from 37% of the GAM forcing at 100 ppmv to 47% at 50,000 ppmv of CO_2). Tables of these forcings are provided for the use of forcing climate models.

For deep paleoclimate, high radiative forcings may be necessary to balance reduced insolation and give a similar climate to today. In other cases though, strong radiative forcing will give climates substantially different from today (both "hothouse" and "icehouse" climates existed). Under such large climate changes, substantial nonsmooth climate feedbacks are expected, and the proportionality between radiative forcing and mean surface temperature will weaken. Such climates are an active area of research with general circulation models [e.g., *Abbot et al.*, 2013; *Russell et al.*, 2013]. Nonetheless, radiative forcings and a climate sensitivity parameter of ≈0.5 K/(W m^{-2}) [*IPCC*, 2001] provide a good first-approximation estimate of climate change and are the best way of comparing the relative efficacy of different greenhouse gases.

Acknowledgments
We thank David Crisp and Ty Robinson for their help with SMART. Financial support was received from the Natural Sciences and Engineering Research Council of Canada (NSERC) CREATE Training Program in Interdisciplinary Climate Science at the University of Victoria (UVic); a University of Victoria graduate fellowship to B.B. and NSERC Discovery grant to C.G. This research has been enabled by the use of computing resources provided by WestGrid and Compute/Calcul Canada.

The Editor thanks two anonymous reviewers for their assistance in evaluating this paper.

References

Abbot, D. S., A. Voigt, D. Li, G. Le Hir, R. T. Pierrehumbert, M. Branson, D. Pollard, and D. D. B. Koll (2013), Robust elements of Snowball Earth atmospheric circulation and oases for life, *J. Geophys. Res. Atmos.*, *118*, 6017–6027, doi:10.1002/jgrd.50540.

Beerling, D., R. A. Berner, F. T. Mackenzie, M. B. Harfoot, and J. A. Pyle (2009), Methane and the CH_4-related greenhouse effect over the past 400 million years, *Am. J. Sci.*, *309*(2), 97–113, doi:10.2475/02.2009.01.

Collins, W. D., et al. (2006), Radiative forcing by well-mixed greenhouse gases: Estimates from climate models in the Intergovernmental Panel on Climate Change (IPCC) Fourth Assessment Report (AR4), *J. Geophys. Res.*, *111*, D14317, doi:10.1029/2005JD006713.

Freckleton, R., E. Highwood, K. Shine, O. Wild, K. Law, and M. Sanderson (1998), Greenhouse gas radiative forcing: Effects of averaging and inhomogeneities in trace gas distribution, *Q. J. R. Meteorolog. Soc.*, *124*(550), 2099–2127, doi:10.1002/qj.49712455014.

Hansen, J., I. Fung, A. Lacis, D. Rind, S. Lebedeff, R. Ruedy, G. Russell, and P. Stone (1988), Global climate changes as forecast by Goddard Institute for space studies three-dimensional model, *J. Geophys. Res.*, *93*(D8), 9341–9364, doi:10.1029/JD093iD08p09341.

Hansen, J., M. Sato, and R. Ruedy (1997), Radiative forcing and climate response, *J. Geophys. Res.*, *102*(D6), 6831–6864, doi:10.1029/96JD03436.

Hansen, J., et al. (2005), Efficacy of climate forcings, *J. Geophys. Res.*, *110*, D18104, doi:10.1029/2005JD005776.

IPCC (1990), *Climate Change: The IPCC Scientific Assessment*, Cambridge Univ. Press, Cambridge, U.K., and New York.

IPCC (2001), *Climate Change 2001: The Scientific Basis. Contribution of Working Group I to the Third Assessment Report of the Intergovernmental Panel on Climate Change*, Cambridge Univ. Press, Cambridge, U. K., and New York.

IPCC (2013), *Climate Change 2013: The Scientific Basis. Contribution of Working Group I to the Fifth Assessment Report of the Intergovernmental Panel on Climate Change*, Cambridge Univ. Press, Cambridge, U. K., and New York.

Kurten, T., et al. (2011), Large methane releases lead to strong aerosol forcing and reduced cloudiness, *Atmos. Chem. Phys.*, *11*(14), 6961–6969, doi:10.5194/acp-11-6961-2011.

Meadows, V., and D. Crisp (1996), Ground-based near-infrared observations of the Venus nightside: The thermal structure and water abundance near the surface, *J. Geophys. Res.*, *101*(E2), 4595–4622, doi:10.1029/95JE03567.

Meinshausen, M., et al. (2011), The RCP greenhouse gas concentrations and their extensions from 1765 to 2300, *Clim. Change*, *109*(1-2, SI), 213–241, doi:10.1007/s10584-011-0156-z.

©2013. American Geophysical Union. All Rights Reserved.

Myhre, G., and F. Stordal (1997), Role of spatial and temporal variations in the computation of radiative forcing and GWP, *J. Geophys. Res.*, *102*(D10), 11,181–11,200, doi:10.1029/97JD00148.
Rienecker, M. M., et al. (2011), MERRA: NASA's modern-era retrospective analysis for research and applications, *J. Clim.*, *24*(14), 3624–3648, doi:10.1175/JCLI-D-11-00015.1.
Rossow, W., Y. Zhang, and J. Wang (2005), A statistical model of cloud vertical structure based on reconciling cloud layer amounts inferred from satellites and radiosonde humidity profiles, *J. Clim.*, *18*(17), 3587–3605, doi:10.1175/JCLI3479.1.
Royer, D. L. (2006), CO_2-forced climate thresholds during the Phanerozoic, *Geochim. Cosmochim. Acta*, *70*(23), 5665–5675, doi:10.1016/j.gca.2005.11.031.
Russell, G. L., A. A. Lacis, D. H. Rind, C. Colose, and R. F. Opstbaum (2013), Fast atmosphere-ocean model runs with large changes in CO_2, *Geophys. Res. Lett.*, *40*, 5787–5792, doi:10.1002/2013GL056755.
Schmidt, G., and D. Shindell (2003), Atmospheric composition, radiative forcing, and climate change as a consequence of a massive methane release from gas hydrates, *Paleoceanography*, *18*(1), 1004, doi:10.1029/2002PA000757.
Shaffer, G., S. M. Olsen, and J. O. P. Pedersen (2008), Presentation, calibration and validation of the low-order, DCESS Earth System Model (Version 1), *Geosci. Model Dev.*, *1*(1), 17–51.
Shi, G. (1992), Radiative forcing and greenhouse effect due to the atmospheric trace gases, *Sci. China, Ser. B Chem.*, *35*, 217–229.
Tachiiri, K., J. C. Hargreaves, J. D. Annan, A. Oka, A. Abe-Ouchi, and M. Kawamiya (2010), Development of a system emulating the global carbon cycle in Earth system models, *Geosci. Model Dev.*, *3*(2), 365–376, doi:10.5194/gmd-3-365-2010.
Weaver, A., et al. (2001), The UVic Earth System Climate Model: Model description, climatology, and applications to past, present and future climates, *Atmos. Ocean*, *39*(4), 361–428.
WMO (1986), Atmospheric ozone 1985 assessment of our understanding of the processes controlling its present distribution and change, *Report No. 16*, Geneva, Switzerland.
WMO (1999), Scientific assessment of ozone depletion: 1998 global ozone research and monitoring project, *Report No. 44*, WMO, Geneva, Switzerland.

Erratum

In the originally published version of this article, in Table 2, several pairs of square brackets were missing. The missing brackets have since been added, and this version may be considered the authoritative version of record.

©2013. American Geophysical Union. All Rights Reserved.